Journal of Physics and Chemistry of Solids 183 (2023) 111653

Contents lists available at ScienceDirect

Journal of Physics and Chemistry of Solids

journal homepage: www.elsevier.com/locate/jpcs

Two-dimensional α-In_2Se_3 field effect transistor for wide-band photodetection and non-volatile memory

Aniello Pelella [a], Kimberly Intonti [b,e], Loredana Viscardi [b,e], Ofelia Durante [b,e], Daniele Capista [c], Maurizio Passacantando [c,d], Filippo Giubileo [e], Paola Romano [a,e], Mohammed Ali S. Alshehri [f], Manal Safar G. Alghamdi [f], Monica Felicia Craciun [f], Saverio Russo [f], Antonio Di Bartolomeo [b,e,*]

[a] Department of Science and Technology, Università degli studi del Sannio, via De Sanctis 59/A, Benevento, 82100, Italy
[b] Department of Physics "E. R. Caianiello", University of Salerno, via Giovanni Paolo II, Fisciano, Salerno, 84084, Italy
[c] Department of Physical and Chemical Science, University of L'Aquila, Via Vetoio, 67100, Coppito, L'Aquila, Italy
[d] CNR-SPIN L'Aquila, Via Vetoio, 67100, Coppito, L'Aquila, Italy
[e] CNR-SPIN Salerno, via Giovanni Paolo II, Fisciano, 84084, Italy
[f] University of Exeter, Stocker Road 6, Exeter, EX4 4QL, Devon, UK

ARTICLE INFO

Keywords:
Field effect transistor
Photodetector
Indium selenide
Data storage
2D material

ABSTRACT

Mechanically exfoliated two-dimensional α-In_2Se_3 flakes are used as the channel material in field effect transistors. N-type conduction with 0.14 $\frac{cm^2}{Vs}$ carrier mobility is reported. The good gate modulation and the pronounced hysteresis make the device suitable for a wide range of applications, from digital logics to memories. An order of magnitude current increase is observed under illumination by a blue light at the incident optical power of 19 nW. The devices can work as visible-to-infrared wide-band photodetectors with time response of few-hundred milliseconds, responsivity up to 40 A/W and specific detectivity $D^* = 5{\cdot}10^{11}$ *Jones* at low light intensity.

1. Introduction

After the discovery of graphene, the interest in two-dimensional (2D) crystals has grown exponentially [1–3]. 2D materials are good candidates for nanoscale electronic and optoelectronic applications and the promising applications have motivated the researchers, in the past years, to investigate their physical properties and to develop new high-performance devices [4–9].

Layered crystals, such as transition metal dichalcogenides [10], group IV-V [11], or group III-VI compounds show strong in-plane covalent bonds and weak interplane van der Waals interactions. Thanks to this peculiar structure, it is easy to obtain monolayers or few layers via chemical vapor deposition (CVD) and mechanical exfoliation from their bulk crystals [12–15].

Indium selenide (In_2Se_3) is a III-VI compound. There are five known crystalline forms (α,β,γ,δ,κ) which differ from each other for lattice parameters and material properties [16–19]. The most common form is α-phase. α-In_2Se_3 is widely used as channel material for field effect transistors [20–23] and several other applications, like photodetection and data storage [24–26].

In_2Se_3 field-effect transistors (FETs) have gained attention due to their unique electronic properties, including high carrier mobility, low noise, and high current density [27–29]. Xiaotian Zhang et al. have reported a mobility of $\sim 1\ cm^2\ V^{-1}\ s^{-1}$ for a few layer β-In_2Se_3 FET [30]. A similar value ($\sim 2.5\ cm^2\ V^{-1}\ s^{-1}$) of mobility has been reported by Jiadong Zhou et al. for a monolayer α-In_2Se_3 FET [31].

In_2Se_3 FETs have shown great promise for use in various applications, including high-speed electronics [32], sensors [33], solar energy harvesting [34], non-volatile phase-change memory [25], and optoelectronics [35].

Due to the combination of a direct band-gap [36], the efficient absorption of light [37] and sensitivity [38], In_2Se_3 photodetectors have been proposed for imaging [39,40], sensing [41], and communication [42] purposes. The 1.3 eV band gap enables absorption of a wide range of photons, making the photodetector suitable for the detection of a wide spectral range [42]. Moreover, In_2Se_3 photodetectors have demonstrated fast response times, with values in the order of 1–100 μs [40,42,43].

In this work, mechanically exfoliated α-In_2Se_3 flakes have been used as the channel material for 2D field effect transistors. α-In_2Se_3 electronic

* Corresponding author. Department of Physics "E. R. Caianiello", University of Salerno, via Giovanni Paolo II, Fisciano, Salerno, 84084, Italy.
E-mail address: adibartolomeo@unisa.it (A. Di Bartolomeo).

https://doi.org/10.1016/j.jpcs.2023.111653
Received 17 May 2023; Received in revised form 23 August 2023; Accepted 6 September 2023
Available online 7 September 2023
0022-3697/© 2023 The Authors. Published by Elsevier Ltd. This is an open access article under the CC BY license (http://creativecommons.org/licenses/by/4.0/).

characteristics have been investigated in FET configuration measuring the current-voltage (I–V) output and transfer curves. We have characterized the optical properties using LEDs with different wavelengths and incident optical power. Finally, we demonstrate the application of In_2Se_3 FETs as memory devices by switching among two stable states by voltage pulses applied to the back gate contact (V_{gs}).

2. Materials and methods

The channel flakes were prepared by mechanical exfoliation technique from bulk In_2Se_3 crystal and then transferred onto a 290 nm SiO_2 doped Si substrate (n-type, As dopant, $\rho \leq 0.005\ \Omega{\cdot}m$). Before transferring the flakes, an Oxygen plasma treatment and an annealing process were used to further clean the substrate. Then, the Cr/Au (5/110 nm) electrodes were patterned by standard Electron Beam Lithography (EBL).

A Scanning Electron Microscopy (SEM) image of a typical device, obtained with a field-emission SEM Zeiss LEO 1530 using an acceleration voltage of 5 kV, is shown in Fig. 1a. The schematic of the device is displayed in Fig. 1b. It consists of interdigitated source/drain metal contacts deposited over the In_2Se_3 flake resulting in a channel length $L = 3.75\ \mu m$ and width $W = 1.85\ \mu m$. The aspect ratio attained in this device has a positive impact on reducing the role of the contact resistance known to have an inverse proportionality to the channel width in the metal/2D materials transistors [44]. In addition, this device configuration maximises the value of the photosensitive area (i.e. $W * L$) in a short channel In_2Se_3 photodetector. Finally, the doped silicon substrate works as a global back-gate.

To investigate the morphology and the thickness of the In_2Se_3 flake, Atomic Force Microscope (AFM) characterization has been performed on several flakes. The AFM images (Fig. 1c) have been acquired with a Nanosurf A.G. Microscope and the data have been analysed with the software WSXM 5.0 Develop 9.4. The AFM profile in Fig. 1d - measured along the solid black line in Fig. 1c -shows that flake thickness is around 11 nm, which corresponds to ~ 10 layers (monolayer thickness is around 1.2 nm) [45,46].

For the optical and electrical characterization, the devices were placed onto the sample holder of a SEM chamber and contacted with two nanoprobes, electrically connected to a Keithley 4200-SCS Semiconductor Parameter Analyzer. The devices were exposed to the light of three LEDs with different wavelengths, directly sent on the surface of the sample.

3. Results and discussion

Fig. 2a shows the $I_{ds} - V_{ds}$ output characteristic on linear scale of the device. It exhibits slightly asymmetric behaviour indicating Schottky contacts at drain and source terminals [47]. This behaviour can be easily explained with either one or two barrier model, as reported elsewhere [48,49].

An applied gate voltage modulates the channel current with a subthreshold swing (SS) around 12 V/dec, as reported in Fig. 2b both on logarithmic (black) and linear (red) scale. SS has been evaluated from the transfer characteristic, i.e. the $I_{ds} - V_{gs}$ plot, as:

$$SS = \left(\frac{d(\log(I_{ds}))}{dV_{gs}}\right)^{-1}$$

The transfer characteristic also indicates that the majority carriers are electrons (n-type behaviour) with a mobility $= 0.14\ cm^2\ V^{-1}s^{-1}$. Electron mobility has been extracted from the transfer characteristic on linear scale using the following equation:

$$\mu = \frac{L}{W}\frac{1}{C_{ox}}\frac{1}{V_{ds}}g_m$$

where L and W are length and width of the channel, $C_{ox} = 1.15x10^{-8}\ F$ is the capacitance of silicon oxide, V_{ds} is the applied drain-source voltage, and $g_m = \frac{dI_{ds}}{dV_{gs}}$ is the maximum transconductance of In_2Se_3.

To test the photoresponse of the device, a blue LED (405 nm) was used to illuminate the channel whilst measuring the output curves. The diameter of the light spot is about 2 mm, and it covers the whole channel flake, i.e. the entire active area (A_{act}). Given $A_{act} = 6.85\ \mu m^2$, the incident optical power is obtained as: $P_{inc} = P * \frac{A_{act}}{Spot\ area}$. The results are

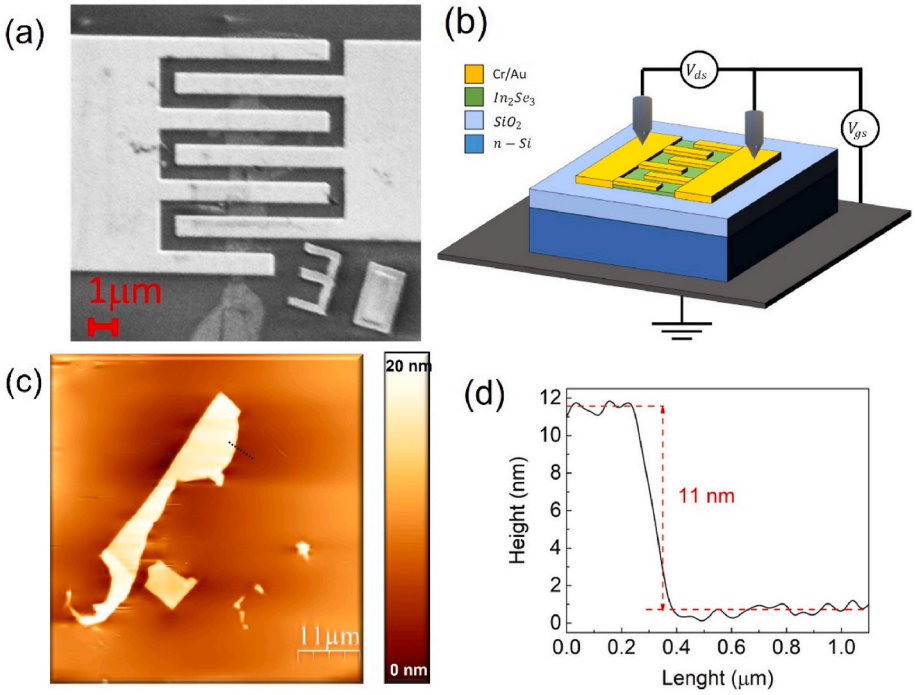

Fig. 1. (a) SEM image and (b) schematic layout of the device under test. AFM (c) image and (d) profile of the In_2Se_3 flake measured along the black dotted line in figure (c).

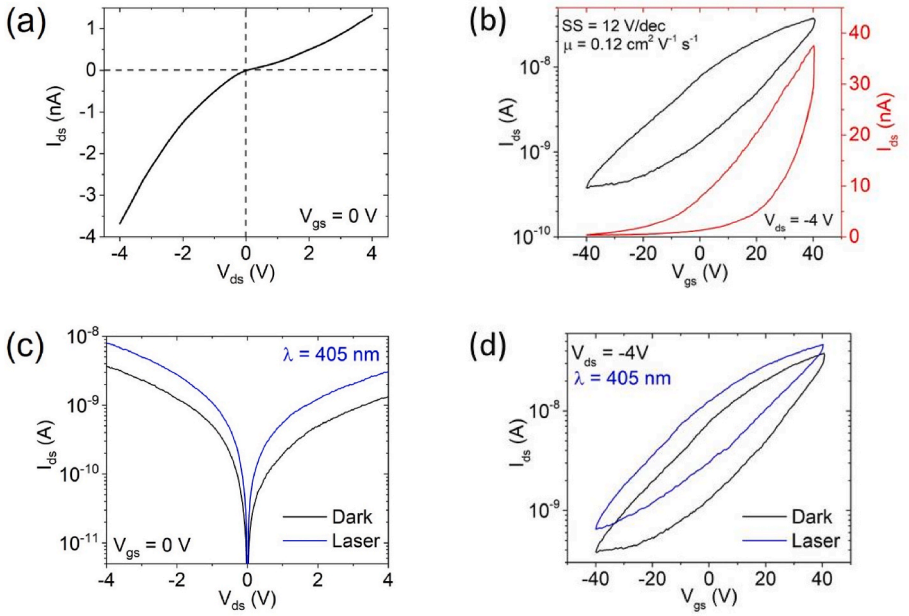

Fig. 2. (a) Current-Voltage characteristic in dark condition and ambient pressure at $V_{gs} = 0\ V$. (b) Transfer characteristic in linear (red) and semi-logarithmic scale (black) in dark condition and $V_{ds} = -4$ V. (c) Current-Voltage characteristics at $V_{gs} = 0\ V$ and (d) transfer characteristics in dark and under blue LED exposure ($\lambda = 405\ nm$) in semi-logarithmic scale.

reported in Fig. 2c. Photogeneration of carriers and carrier detrapping occur upon illuminating the semiconducting channel, thus resulting in an increase of the source-drain current (photocurrent). The light irradiation also affects the transfer characteristic (Fig. 2d), resulting in a left shift of the threshold voltage due to a photogating effect resulting from trapping of the photogenerated positive charges at the interface In_2Se_3/SiO_2 and desorption of physiosorbed Oxygen [35,50–53].

To further investigate the optical properties of the device, a series of light pulses with different light intensity has been applied. The light source power (P) has been increased up to about 12 mW and then successively decreased to zero. The result is displayed in Fig. 3a, in which the device - biased at $V_{ds} = 2\ V$ and $V_{gs} = 0\ V$ - was exposed to two sequences of light pulses of increasing (P_{inc} from 24 pW to 19 nW) and decreasing (P_{inc} from 19 nW to 24 pW) intensity, respectively.

Fig. 3a shows a plot of the time dependent photocurrent measured in the device in dark (i.e. low photocurrent level) and upon illumination for varying incident optical power (i.e. high photocurrent level). A plot of the measured photocurrent ($I_{ph} = I_{light} - I_{dark}$) as a function of the incident optical power reveals a power law dependence of I_{ph} due to the photogeneration rate of the excess charge carriers, which varies with the charge carrier density, see Fig. 3b [54]. The increase of the incident optical power leads to an increase in photogenerated charge carriers and

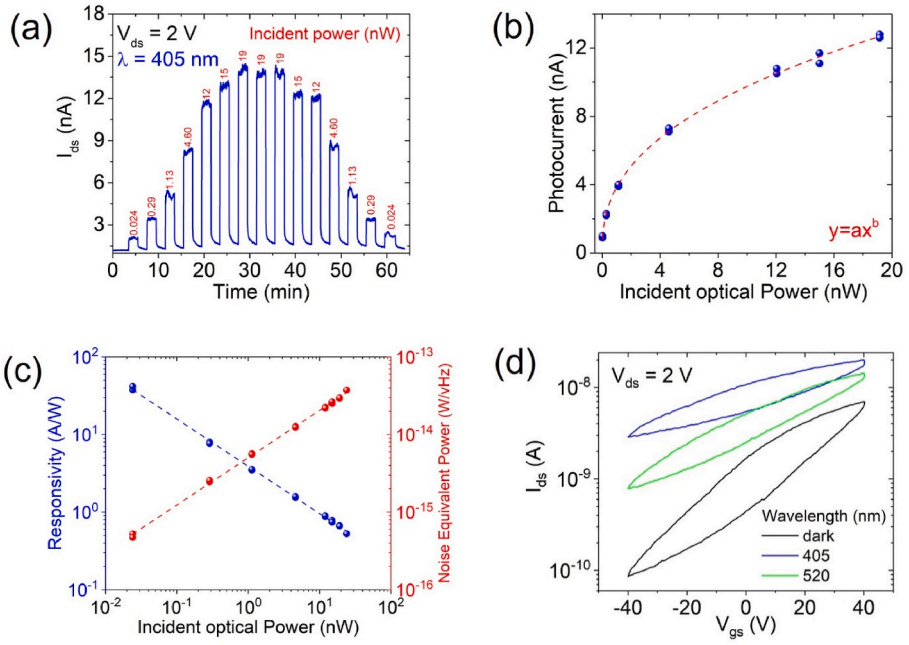

Fig. 3. (a) Current peaks obtained with different optical incident power. (b) Photocurrent at different incident light power extracted from data in Fig. 3a. (c) Responsivity and NEP versus incident light power, and (d) transfer characteristics for light at different wavelengths.

consequently an increase in photocurrent. The higher charge carrier density results in an increased recombination rate as well as in increased scattering rate. Both effects, limit the rate at which the photocurrent increases under stronger illumination. Fig. 3c shows the responsivity of the device, defined as $R = \frac{I_{ph}}{P_{inc}}$. The responsivity decreases at high incident optical power, when the enhanced carrier density leads to an increase of scattering rate favouring electron-hole recombination [55]. Besides, the optical Noise Equivalent Power (NEP) of the device, defined as $NEP = \frac{\sqrt{2qI_{dark}}}{R}$, is reported on the right y-axis of Fig. 3c. A smaller optical NEP is found at low power, indicating that the device is more sensitive when the incident light power is reduced. The lowest value of NEP ($5 \cdot 10^{-16}\ W/\sqrt{Hz}$) is achieved at low power, corresponding to a specific detectivity $D^* = R\sqrt{A_{act}/2qI_{dark}} = 5 \cdot 10^{11}$ *Jones*. The photodetector performance ranks among the highest found in the literature [41, 56–58].

Moreover, the device performance has been tested at different wavelength of the incident light. The transfer characteristics of the device irradiated by different wavelengths are displayed in Fig. 3d. The photocurrent (and thus the device responsivity) varies at different wavelengths. Also, the left shift of the threshold voltage decreases with decreasing responsivity, in totally agreement of the already mentioned photogating effect.

Fig. 4a shows current peaks generated by three LEDs with different wavelength (same incident optical power Pinc≃4 nW), namely blue (λ = 405 nm), green (λ = 520 nm) and infrared (λ = 880 nm). Peaks analysis have been performed on three peaks from the three different incident wavelengths (Fig. 4b–d). The data have been fitted with a double-exponential formula $\left(y = Aexp\left(-\frac{x}{t_1}\right) + Bexp\left(-\frac{x}{t_2}\right)\right)$ which gives two different time constants for each rising and falling edges [59]. Double-exponential formula is needed for taking into account for two different mechanisms: (1) low time constants correspond to the standard carriers photogeneration process and the consequent increase of current through the channel. (2) high time constants, instead, describe the absorption/desorption of adsorbates, such as water and oxygen molecules, activated by the incidence of the light source onto the In_2Se_3 channel.

Finally, we show that the wide hysteresis in the transfer characteristics, which is reproducible and common to other 2D materials based devices, can be exploited in a data storage device [3,7,60,61]. A sequence of write/read/erase/read memory cycles is displayed in Fig. 5a. Voltage pulses are applied at the back gate ($V_{gs} = \pm 40\ V$) for the write and erase operations and the read is performed at $V_{gs} = 0\ V$ while the channel current is monitored. The data show two different current states (I_{up} and I_{down}, Fig. 4b) which can be swapped among each other by applying the write/erase pulses. The rising and falling edges of the curves in Fig. 4b have been fitted with an exponential law to extract time constants and to ensure that I_{up} and I_{down} are well separated. Time constants are in the order of the seconds, which is consistent with other works on similar 2D data storage devices [62–64]. Besides, we demonstrated that the device shows a retention time i.e., the time the current stays in the low/high state, longer than 50 s.

Finally, the resistance states R_{down} and R_{up}, corresponding to the current states I_{up} and I_{down} and to 0 and 1 logic states, present a resistance window $\frac{\Delta R}{R_{mean}} = \frac{R_{up} - R_{down}}{(R_{up} + R_{down})/2}$ of ∼ 68%, confirming the device has two well distinguishable memory states (Fig. 5c).

4. Conclusions

A detailed optoelectronic characterization of α-In_2Se_3 field effect transistors has been reported, showing carrier mobility of 0.14 $cm^2\ V^{-1}s^{-1}$ and subthreshold swing of 12 V/dec in dark conditions. The device shows high performance as photodetector, with a responsivity up to 40 A/W and a specific detectivity of $5 \cdot 10^{11}$ *Jones*. It can also work in the infrared region, making it a good candidate for optical communication. Moreover, thanks to the wide hysteresis shown in its transfer characteristic, the device can operate as a memory. Indeed, we have demonstrated two different resistance logic states which can be easily selected by applying opposite gate voltage pulses.

Author statement

Aniello Pelella, Antonio Di Bartolomeo: Conceptualization, Methodology, Investigation, Writing - Original Draft, Supervision, Funding acquisition. Kimberly Intonti, Loredana Viscardi, Ofelia Durante, Daniele Capista, Mohammed Ali S Alshehri, Manal Safar G Alghamdi:

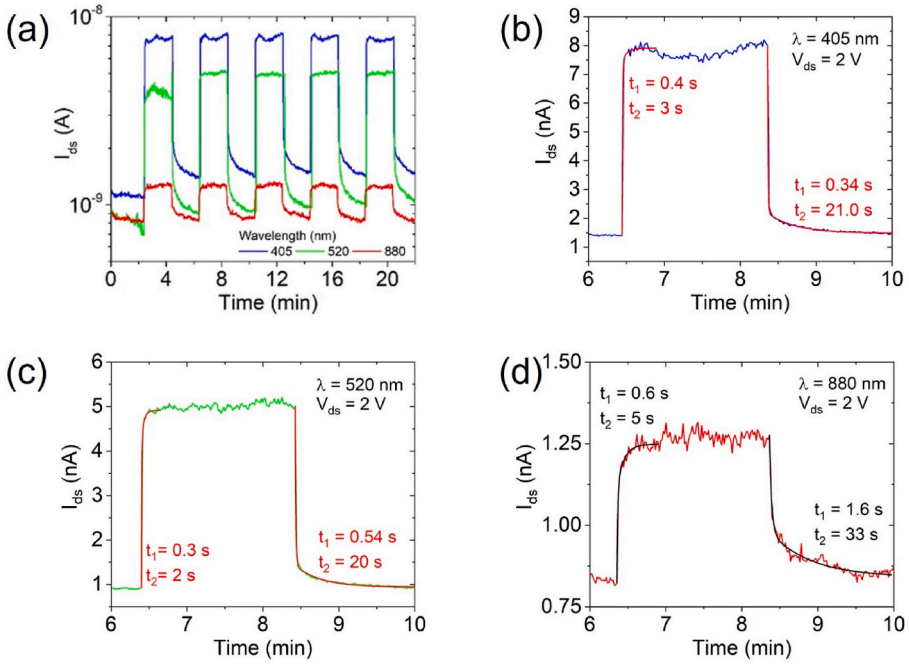

Fig. 4. (a) Current peaks obtained at different wavelengths. Extraction of time responses of the device irradiated by (b) blue, (c) green and (d) IR LED.

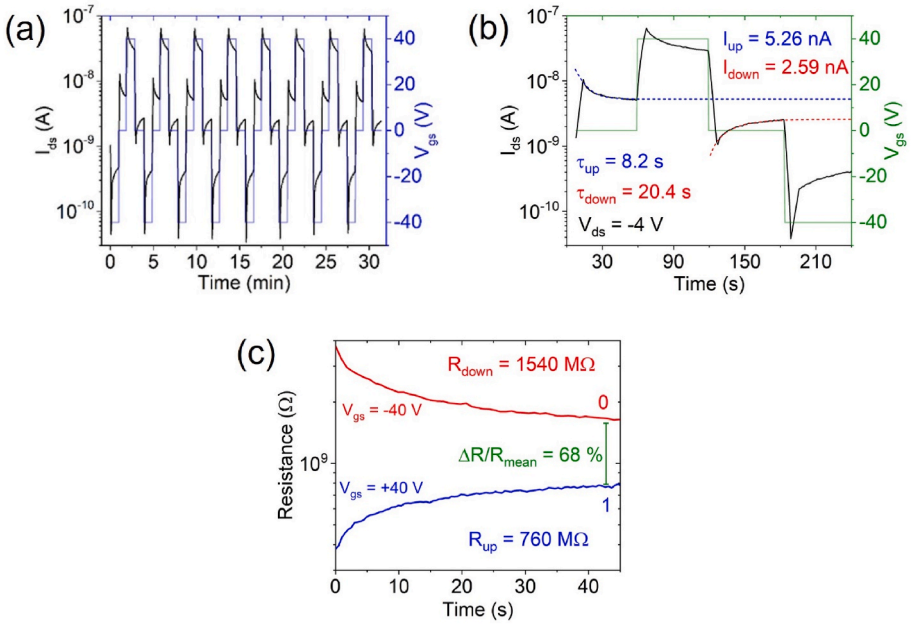

Fig. 5. (a) Write/read/erase/read memory cycles. (b) Detail of a single memory cycle with evaluation of time constants and current states from a peak current analysis. (c) Evaluation of the resistance window between R_{up} and R_{down}.

Software, Data curation, Investigation, Validation. Paola Romano, Maurizio Passacantando, Filippo Giubileo: Visualization, Investigation, Validation, Writing- Reviewing and Editing. Monica Felicia Craciun, Saverio Russo: Resources, Writing- Reviewing and Editing, Funding acquisition.

Declaration of competing interest

The authors declare that they have no known competing financial interests or personal relationships that could have appeared to influence the work reported in this paper.

Data availability

Data will be made available on request.

Acknowledgments

M.S.G.A. acknowledges financial support from the Physics Department-Faculty of Sciences-Al-Baha University-Al-Baha-Saudi Arabia, M.A.S.A. acknowledges financial support from the Physics Department-Faculty of Sciences-King Abdulaziz University-Jeddah-Saudi Arabia, S.R. and M.F.C. acknowledge financial support from EPSRC (EP/V048163/1 and EP/V052306/1) and the Leverhulme trust, A.D.B. acknowledges financial support from the University of Salerno with grant ORSA223384.

References

[1] A.K. Geim, K.S. Novoselov, The rise of graphene, Nat. Mater. 6 (2007) 183–191, https://doi.org/10.1038/nmat1849.
[2] A. Di Bartolomeo, Emerging 2D materials and their van der Waals heterostructures, Nanomaterials 10 (2020) 579, https://doi.org/10.3390/nano10030579.
[3] A. Grillo, A. Pelella, E. Faella, F. Giubileo, S. Sleziona, O. Kharsah, M. Schleberger, A.D. Bartolomeo, Memory effects in black phosphorus field effect transistors, 2D Mater. 9 (2021), 015028, https://doi.org/10.1088/2053-1583/ac3f45.
[4] M.C. Lemme, D. Akinwande, C. Huyghebaert, C. Stampfer, 2D materials for future heterogeneous electronics, Nat. Commun. 13 (2022) 1392, https://doi.org/10.1038/s41467-022-29001-4.
[5] S. Das, A. Sebastian, E. Pop, C.J. McClellan, A.D. Franklin, T. Grasser, T. Knobloch, Y. Illarionov, A.V. Penumatcha, J. Appenzeller, Z. Chen, W. Zhu, I. Asselberghs, L.-J. Li, U.E. Avci, N. Bhat, T.D. Anthopoulos, R. Singh, Transistors based on two-dimensional materials for future integrated circuits, Nat Electron 4 (2021) 786–799, https://doi.org/10.1038/s41928-021-00670-1.
[6] A. Pelella, D. Capista, M. Passacantando, E. Faella, A. Grillo, F. Giubileo, N. Martucciello, A. Di Bartolomeo, A self-powered CNT–Si photodetector with tuneable photocurrent, Adv. Electronic Mater. 9 (2023), 2200919, https://doi.org/10.1002/aelm.202200919.
[7] A. Kumar, L. Viscardi, E. Faella, F. Giubileo, K. Intonti, A. Pelella, S. Sleziona, O. Kharsah, M. Schleberger, A.D. Bartolomeo, Temperature dependent black phosphorus transistor and memory, Nano Ex 4 (2023), 014001, https://doi.org/10.1088/2632-959X/acbe11.
[8] J. An, X. Zhao, Y. Zhang, M. Liu, J. Yuan, X. Sun, Z. Zhang, B. Wang, S. Li, D. Li, Perspectives of 2D materials for optoelectronic integration, Adv. Funct. Mater. 32 (2022), 2110119, https://doi.org/10.1002/adfm.202110119.
[9] F. Urban, G. Lupina, A. Grillo, N. Martucciello, A. Di Bartolomeo, Contact resistance and mobility in back-gate graphene transistors, Nano Ex 1 (2020), 010001, https://doi.org/10.1088/2632-959X/ab7055.
[10] S. Manzeli, D. Ovchinnikov, D. Pasquier, O.V. Yazyev, A. Kis, 2D transition metal dichalcogenides, Nat. Rev. Mater. 2 (2017) 1–15, https://doi.org/10.1038/natrevmats.2017.33.
[11] A. Grillo, A. Di Bartolomeo, F. Urban, M. Passacantando, J.M. Caridad, J. Sun, L. Camilli, Observation of 2D conduction in ultrathin germanium arsenide field-effect transistors, ACS Appl. Mater. Interfaces 12 (2020) 12998–13004, https://doi.org/10.1021/acsami.0c00348.
[12] J. Shim, H.-Y. Park, D.-H. Kang, J.-O. Kim, S.-H. Jo, Y. Park, J.-H. Park, Electronic and optoelectronic devices based on two-dimensional materials: from fabrication to application, Adv. Electron. Mater. 3 (2017), 1600364, https://doi.org/10.1002/aelm.201600364.
[13] Q. Zhang, L. Mei, X. Cao, Y. Tang, Z. Zeng, Intercalation and exfoliation chemistries of transition metal dichalcogenides, J. Mater. Chem. A 8 (2020) 15417–15444, https://doi.org/10.1039/D0TA03727C.
[14] B. Zhao, D. Shen, Z. Zhang, P. Lu, M. Hossain, J. Li, B. Li, X. Duan, 2D metallic transition-metal dichalcogenides: structures, synthesis, properties, and applications, Adv. Funct. Mater. 31 (2021), 2105132, https://doi.org/10.1002/adfm.202105132.
[15] X. Song, Z. Guo, Q. Zhang, P. Zhou, W. Bao, D.W. Zhang, Progress of large-scale synthesis and electronic device application of two-dimensional transition metal dichalcogenides, Small 13 (2017), 1700098, https://doi.org/10.1002/smll.201700098.
[16] S. Mukherjee, E. Koren, Indium selenide (In2Se3) – an emerging van-der-waals material for photodetection and non-volatile memory applications, Isr. J. Chem. 62 (2022), e202100112, https://doi.org/10.1002/ijch.202100112.
[17] D.W. Boukhvalov, B. Gürbulak, S. Duman, L. Wang, A. Politano, L.S. Caputi, G. Chiarello, A. Cupolillo, The advent of indium selenide: synthesis, electronic properties, ambient stability and applications, Nanomaterials 7 (2017) 372, https://doi.org/10.3390/nano7110372.
[18] G. Han, Z.-G. Chen, J. Drennan, J. Zou, Indium selenides: structural characteristics, synthesis and their thermoelectric performances, Small 10 (2014) 2747–2765, https://doi.org/10.1002/smll.201400104.
[19] A. Politano, D. Campi, M. Cattelan, I. Ben Amara, S. Jaziri, A. Mazzotti, A. Barinov, B. Gürbulak, S. Duman, S. Agnoli, L.S. Caputi, G. Granozzi, A. Cupolillo, Indium

selenide: an insight into electronic band structure and surface excitations, Sci. Rep. 7 (2017) 3445, https://doi.org/10.1038/s41598-017-03186-x.
[20] M. Si, A.K. Saha, S. Gao, G. Qiu, J. Qin, Y. Duan, J. Jian, C. Niu, H. Wang, W. Wu, S. K. Gupta, P.D. Ye, A ferroelectric semiconductor field-effect transistor, Nat Electron 2 (2019) 580–586, https://doi.org/10.1038/s41928-019-0338-7.
[21] M. Soleimani, N. Asoudegi, P. Khakbaz, M. Pourfath, Negative capacitance field-effect transistor based on a two-dimensional ferroelectric, in: 2019 International Conference on Simulation of Semiconductor Processes and Devices, SISPAD, 2019, pp. 1–4, https://doi.org/10.1109/SISPAD.2019.8870372.
[22] Y. Li, M. Gong, H. Zeng, Atomically thin α-In2Se3: an emergent two-dimensional room temperature ferroelectric semiconductor, J. Semiconduct. 40 (2019), 061002, https://doi.org/10.1088/1674-4926/40/6/061002.
[23] Q. He, Z. Tang, M. Dai, H. Shan, H. Yang, Y. Zhang, X. Luo, Epitaxial growth of large area two-dimensional ferroelectric α-In2Se3, Nano Lett. 23 (2023) 3098–3105, https://doi.org/10.1021/acs.nanolett.2c04289.
[24] B. Tang, X. Li, J. Liao, Q. Chen, Ultralow power consumption and large dynamic range synaptic transistor based on α-In2Se3 nanosheets, ACS Appl. Electron. Mater. 4 (2022) 598–605, https://doi.org/10.1021/acsaelm.1c00970.
[25] S. Wan, Y. Li, W. Li, X. Mao, C. Wang, C. Chen, J. Dong, A. Nie, J. Xiang, Z. Liu, W. Zhu, H. Zeng, Ferroelectrics: nonvolatile ferroelectric memory effect in ultrathin α-In2Se3 (Adv. Funct. Mater. 20/2019), Adv. Funct. Mater. 29 (2019), 1970136, https://doi.org/10.1002/adfm.201970136.
[26] P. Hou, Y. Lv, Y. Chen, Y. Liu, C. Wang, P. Zhou, X. Zhong, J. Wang, X. Ouyang, In-plane strain-modulated photoresponsivity of the α-In2Se3-based flexible transistor, ACS Appl. Electron. Mater. 2 (2020) 140–146, https://doi.org/10.1021/acsaelm.9b00658.
[27] Y. Li, C. Chen, W. Li, X. Mao, H. Liu, J. Xiang, A. Nie, Z. Liu, W. Zhu, H. Zeng, Orthogonal electric control of the out-of-plane field-effect in 2D ferroelectric α-In2Se3, Advanced Electronic Materials 6 (2020), 2000061, https://doi.org/10.1002/aelm.202000061.
[28] E.F. Procopio, N. N Batista, F.A. L de Souza, W.S. Paz, J.J. Palacios, W.L. Scopel, Emergence of topological edge states in oxidized α-in2Se3 nanosheets: implications for field-effect transistors, ACS Appl. Nano Mater. 4 (2021) 8154–8161, https://doi.org/10.1021/acsanm.1c01394.
[29] J.Y. Yang, M.J. Yeom, Y. Park, J. Heo, G. Yoo, Ferroelectric α-In2Se3 wrapped-gate β-Ga2O3 field-effect transistors for dynamic threshold voltage control, Advanced Electronic Materials 7 (2021), 2100306, https://doi.org/10.1002/aelm.202100306.
[30] X. Zhang, S. Lee, A. Bansal, F. Zhang, M. Terrones, T.N. Jackson, J.M. Redwing, Epitaxial growth of few-layer β-In2Se3 thin films by metalorganic chemical vapor deposition, J. Cryst. Growth 533 (2020), 125471, https://doi.org/10.1016/j.jcrysgro.2019.125471.
[31] J. Zhou, Q. Zeng, D. Lv, L. Sun, L. Niu, W. Fu, F. Liu, Z. Shen, C. Jin, Z. Liu, Controlled synthesis of high-quality monolayered α-In2Se3 via physical vapor deposition, Nano Lett. 15 (2015) 6400–6405, https://doi.org/10.1021/acs.nanolett.5b01590.
[32] Y. Zhang, L. Wang, H. Chen, T. Ma, X. Lu, K.P. Loh, Analog and digital mode α-In2Se3 memristive devices for neuromorphic and memory applications, Advanced Electronic Materials 7 (2021), 2100609, https://doi.org/10.1002/aelm.202100609.
[33] X. Zhang, Y. Wu, X. Wang, X. Zhong, J. Wang, Y. Zhang, Realization of a flexible humidity sensor based on α-In2Se3 nanosheets, ChemNanoMat 8 (2022), e202100394, https://doi.org/10.1002/cnma.202100394.
[34] L. Kang, L. Shen, Y.J. Chen, S.C. Sun, X. Gu, H.J. Zheng, Z.K. Liu, J.X. Wu, H. L. Peng, F.W. Zheng, P. Zhang, L.X. Yang, Y.L. Chen, Surface photovoltaic effect and electronic structure of \ensuremath{\beta}-InSe, Phys. Rev. Mater. 4 (2020), 124604, https://doi.org/10.1103/PhysRevMaterials.4.124604.
[35] A. Abderrahmane, C. Woo, P.J. Ko, Tunable optoelectronic properties of a two-dimensional graphene/α-In2Se3/graphene-based ferroelectric semiconductor field-effect transistor, J. Mater. Sci. Mater. Electron. 32 (2021) 20252–20258, https://doi.org/10.1007/s10854-021-06528-8.
[36] F. Lyu, Y. Sun, Q. Yang, B. Tang, M. Li, Z. Li, M. Sun, P. Gao, L.-H. Ye, Q. Chen, Thickness-dependent band gap of α-In2Se3: from electron energy loss spectroscopy to density functional theory calculations, Nanotechnology 31 (2020), 315711, https://doi.org/10.1088/1361-6528/ab8998.
[37] Z. Liu, J. Wu, J. Li, In-plane anisotropic electronic properties in layered α′-In2Se3, J. Appl. Phys. 130 (2021), 015103, https://doi.org/10.1063/5.0050979.
[38] W. Feng, W. Zheng, F. Gao, X. Chen, G. Liu, T. Hasan, W. Cao, P. Hu, Sensitive electronic-skin strain sensor array based on the patterned two-dimensional α-in2Se3, Chem. Mater. 28 (2016) 4278–4283, https://doi.org/10.1021/acs.chemmater.6b01073.
[39] Z. Chen, W. Fu, L. Wang, W. Yu, H. Li, C.K.Y. Tan, I. Abdelwahab, Y. Shao, C. Su, M. Sun, B. Huang, K.P. Loh, Atomic imaging of electrically switchable striped domains in β′-In2Se3, Adv. Sci. 8 (2021), 2100713, https://doi.org/10.1002/advs.202100713.
[40] C.-Y. Wu, J.-W. Kang, B. Wang, H.-N. Zhu, Z.-J. Li, S.-R. Chen, L. Wang, W.-H. Yang, C. Xie, L.-B. Luo, Defect-induced broadband photodetection of layered γ-In2Se3 nanofilm and its application in near infrared image sensors, J. Mater. Chem. C 7 (2019) 11532–11539, https://doi.org/10.1039/C9TC04322E.
[41] M. Anandan, H.-F. Hsieh, F.-C. Liu, C.-Y. Chen, K.-Y. Lee, L.-C. Chao, C.-H. Ho, R.-S. Chen, High-responsivity broad-band sensing and photoconduction mechanism in direct-Gap α-In2Se3 nanosheet photodetectors, Nanotechnology 31 (2020), 465201, https://doi.org/10.1088/1361-6528/abac7e.
[42] J. Zou, Y. Ke, X. Zhou, Y. Huang, W. Du, L. Lin, S. Wei, L. Luo, H. Liu, C. Li, K. Shen, A. Ren, J. Wu, Broadband Visible−Near infrared two-dimensional WSe2/In2Se3 photodetector for underwater optical communications, Adv. Opt. Mater. 10 (2022), 2200143, https://doi.org/10.1002/adom.202200143.
[43] H. Guo, Y. Xia, Y. Yu, R. Zhou, H. Niu, X. Mao, L. Wan, J. Xu, High-speed and broadband spectral photodetectors based on β-In2Se3/Si heterojunction, Mater. Sci. Semicond. Process. 138 (2022), 106304, https://doi.org/10.1016/j.mssp.2021.106304.
[44] S. Russo, M.F. Craciun, M. Yamamoto, A.F. Morpurgo, S. Tarucha, Contact resistance in graphene-based devices, Phys. E Low-dimens. Syst. Nanostruct. 42 (2010) 677–679, https://doi.org/10.1016/j.physe.2009.11.080.
[45] F. Xue, W. Hu, K.-C. Lee, L.-S. Lu, J. Zhang, H.-L. Tang, A. Han, W.-T. Hsu, S. Tu, W.-H. Chang, C.-H. Lien, J.-H. He, Z. Zhang, L.-J. Li, X. Zhang, Room-Temperature ferroelectricity in hexagonally layered α-In2Se3 nanoflakes down to the monolayer limit, Adv. Funct. Mater. 28 (2018), 1803738, https://doi.org/10.1002/adfm.201803738.
[46] Y. Zhou, D. Wu, Y. Zhu, Y. Cho, Q. He, X. Yang, K. Herrera, Z. Chu, Y. Han, M. C. Downer, H. Peng, K. Lai, Out-of-Plane piezoelectricity and ferroelectricity in layered α-In2Se3 nanoflakes, Nano Lett. 17 (2017) 5508–5513, https://doi.org/10.1021/acs.nanolett.7b02198.
[47] B. Liu, F. Lyu, B. Tang, X. Li, J. Liao, Q. Chen, Contact properties of two-dimensional ferroelectric α-In2Se3, ACS Appl. Electron. Mater. (2021), https://doi.org/10.1021/acsaelm.1c00724.
[48] A. Di Bartolomeo, A. Grillo, F. Urban, L. Iemmo, F. Giubileo, G. Luongo, G. Amato, L. Croin, L. Sun, S.-J. Liang, L.K. Ang, Asymmetric Schottky contacts in bilayer MoS2 field effect transistors, Adv. Funct. Mater. 28 (2018), 1800657, https://doi.org/10.1002/adfm.201800657.
[49] A. Grillo, A. Di Bartolomeo, A current–voltage model for double Schottky barrier devices, Adv. Electron. Mater. 7 (2021), 2000979, https://doi.org/10.1002/aelm.202000979.
[50] A.D. Bartolomeo, L. Genovese, T. Foller, F. Giubileo, G. Luongo, L. Croin, S.-J. Liang, L.K. Ang, M. Schleberger, Electrical transport and persistent photoconductivity in monolayer MoS2 phototransistors, Nanotechnology 28 (2017), 214002, https://doi.org/10.1088/1361-6528/aa6d98.
[51] F. Urban, F. Giubileo, A. Grillo, L. Iemmo, G. Luongo, M. Passacantando, T. Foller, L. Madauß, E. Pollmann, M.P. Geller, D. Oing, M. Schleberger, A. Di Bartolomeo, Gas dependent hysteresis in MoS $_2$ field effect transistors, 2D Mater. 6 (2019), 045049, https://doi.org/10.1088/2053-1583/ab4020.
[52] A. Di Bartolomeo, A. Pelella, X. Liu, F. Miao, M. Passacantando, F. Giubileo, A. Grillo, L. Iemmo, F. Urban, S. Liang, Pressure-tunable ambipolar conduction and hysteresis in thin palladium diselenide field effect transistors, Adv. Funct. Mater. 29 (2019), 1902483, https://doi.org/10.1002/adfm.201902483.
[53] J.O. Island, S.I. Blanter, M. Buscema, H.S.J. van der Zant, A. Castellanos-Gomez, Gate controlled photocurrent generation mechanisms in high-gain In2Se3 phototransistors, Nano Lett. 15 (2015) 7853–7858, https://doi.org/10.1021/acs.nanolett.5b02523.
[54] P. Bhattacharya, Semiconductor Optoelectronic Devices, Prentice Hall, 1994.
[55] J.P. Banerjee, S. Banerjee, Physics of Semiconductors and Nanostructures, Taylor & Francis, 2015.
[56] R.B. Jacobs-Gedrim, M. Shanmugam, N. Jain, C.A. Durcan, M.T. Murphy, T. M. Murray, R.J. Matyi, R.L.I. Moore, B. Yu, Extraordinary photoresponse in two-dimensional In2Se3 nanosheets, ACS Nano 8 (2014) 514–521, https://doi.org/10.1021/nn405037s.
[57] W. Feng, F. Gao, Y. Hu, M. Dai, H. Li, L. Wang, P. Hu, High-performance and flexible photodetectors based on chemical vapor deposition grown two-dimensional In2Se3 nanosheets, Nanotechnology 29 (2018), 445205, https://doi.org/10.1088/1361-6528/aadc73.
[58] Q.L. Li, Y. Li, J. Gao, S.D. Wang, X.H. Sun, High performance single In2Se3 nanowire photodetector, Appl. Phys. Lett. 99 (2011), 243105, https://doi.org/10.1063/1.3669513.
[59] A. Di Bartolomeo, A. Kumar, O. Durante, A. Sessa, E. Faella, L. Viscardi, K. Intonti, F. Giubileo, N. Martucciello, P. Romano, S. Sleziona, M. Schleberger, Temperature-dependent photoconductivity in two-dimensional MoS2 transistors, Materials Today Nano 24 (2023), 100382, https://doi.org/10.1016/j.mtnano.2023.100382.
[60] A. Di Bartolomeo, H. Rücker, P. Schley, A. Fox, S. Lischke, K.-Y. Na, A single-poly EEPROM cell for embedded memory applications, Solid State Electron. 53 (2009) 644–648, https://doi.org/10.1016/j.sse.2009.04.007.
[61] K. Intonti, E. Faella, L. Viscardi, A. Kumar, O. Durante, F. Giubileo, M. Passacantando, H.T. Lam, K. Anastasiou, M.F. Craciun, S. Russo, A. Di Bartolomeo, Hysteresis and photoconductivity of few-layer ReSe $_2$ field effect transistors enhanced by air pressure, Adv Elect Materials 9 (2023), 2300066, https://doi.org/10.1002/aelm.202300066.
[62] L. Viscardi, K. Intonti, A. Kumar, E. Faella, A. Pelella, F. Giubileo, S. Sleziona, O. Kharsah, M. Schleberger, A. Di Bartolomeo, Black Phosphorus Nanosheets in Field Effect Transistors with Ni and NiCr Contacts, Phys. Status Solidi. n/a (n.d.) 2200537. https://doi.org/10.1002/pssb.202200537..
[63] A. Kumar, L. Viscardi, E. Faella, F. Giubileo, K. Intonti, A. Pelella, S. Sleziona, O. Kharsah, M. Schleberger, A. Di Bartolomeo, Black phosphorus unipolar transistor, memory, and photodetector, J. Mater. Sci. 58 (2023) 2689–2699, https://doi.org/10.1007/s10853-023-08169-0.
[64] A. Kumar, E. Faella, O. Durante, F. Giubileo, A. Pelella, L. Viscardi, K. Intonti, S. Sleziona, M. Schleberger, A. Di Bartolomeo, Optoelectronic memory in 2D MoS2 field effect transistor, J. Phys. Chem. Solid. (2023), 111406, https://doi.org/10.1016/j.jpcs.2023.111406.